Anisotropic antiferromagnetic order in the spin-orbit coupled trigonal-lattice $Ca_2Sr_2IrO_6$

Jieming Sheng,[1,2] Feng Ye,[2,*] Christina Hoffmann,[2] Valentino R. Cooper,[3] Satoshi Okamoto,[3] Jasminka Terzic,[4,†] Hao Zheng,[4] Hengdi Zhao,[4] and G. Cao[4]

[1]*Department of Physics, Renmin University of China, Beijing 100872, China*

[2]*Neutron Scattering Division, Oak Ridge National Laboratory, Oak Ridge, Tennessee 37831, USA*

[3]*Materials Science and Technology Division, Oak Ridge National Laboratory, Oak Ridge, Tennessee 37831, USA*

[4]*Department of Physics, University of Colorado at Boulder, Boulder, Colorado 80309, USA*

(Received 15 March 2018; revised manuscript received 5 May 2018; published 11 June 2018)

We used single-crystal x-ray and neutron diffraction to investigate the crystal and magnetic structures of trigonal lattice iridate $Ca_2Sr_2IrO_6$. The crystal structure is determined to be $R\bar{3}$ with two distinct Ir sites. The system exhibits long-range antiferromagnetic order below $T_N = 13.1$ K. The magnetic wave vector is identified as (0,0.5,1) with ferromagnetic coupling along the a axis and antiferromagnetic correlation along the b axis. Spins align dominantly within the basal plane along the [1,2,0] direction and tilt 34° toward the c axis. The ordered moment is 0.66(3) μ_B/Ir, larger than other iridates where iridium ions form corner- or edge-sharing IrO_6 octahedral networks. The tilting angle is reduced to ≈19° when a magnetic field of 4.9 T is applied along the c axis. Density functional theory calculations confirm that the experimentally determined magnetic configuration is the most probable ground state with an insulating gap ∼0.5 eV.

DOI: 10.1103/PhysRevB.97.235116

I. INTRODUCTION

Controlling the balance between spin-orbit interactions (SOI), on-site Coulomb interactions, and crystalline electric field splitting in 5*d* iridates is the central theme behind searching for novel quantum phenomena such as $j_{\rm eff} = 1/2$ Mott insulating states [1–3], correlated topological insulators [4,5], spin-liquid phases [6], superconductivity [7,8], and Kitaev models [9–11]. Due to the entangled spin and orbital degrees of freedom, the form of magnetic interactions is no longer dictated by a global spin SU(2) symmetry. This leads to physics that is dramatically different from the 3*d* systems where SOI is of a perturbative nature. The wave functions are composed by the superposition of different orbital and spin states, and the resulting magnetic interactions depend critically on the lattice symmetry. In the case of a 180° Ir-O-Ir bond, the Hamiltonian is governed by an isotropic Heisenberg term plus a weak dipolar-like anisotropy term due to Hund's coupling, while for a 90° bond the anisotropic term due to the off-diagonal hopping matrix results in a quantum analog of the compass model [9]. The strong SOI limit also assumes local cubic symmetry of the IrO_6 octahedra, which is rare in real materials. It was discovered that nearly all iridate families have a certain degree of noncubic distortions. For example, the O-Ir-O bond angle in pyrochlores $R_2Ir_2O_7$ (R denotes rare earth) is an average 6°–10° away from 90° [12], a substantial elongation (tetragonal distortion) of the IrO_6 octahedra occurs in the $j_{\rm eff} = 1/2$ Mott insulator Sr_2IrO_4 [13], and an appreciable trigonal distortion was revealed in a honeycomb lattice Na_2IrO_3 with O-Ir-O bond angles ∼4°–9° deviating from the cubic case [14,15]. Although it was claimed that the $j_{\rm eff} = 1/2$ state is robust against distortion, recent resonant inelastic x-ray scattering (RIXS) studies have shown that the distortion of IrO_6 octahedra leads to a modification of the isotropic wave functions [16,17]. This underscores the need for extending the $j_{\rm eff} = 1/2$ picture to correctly describe the Mott insulating ground states.

In this paper, we report a single-crystal x-ray and neutron diffraction investigation of a trigonal lattice iridate $Ca_2Sr_2IrO_6$ (CSIO). The crystal orders antiferromagnetically (AFM) below 13.1 K with no structural anomaly across the transition. The wave vector of the spin structure is (0,0.5,1), indicating strong anisotropic magnetic interactions. The iridium moments align nearly along the diagonal O-Ir-O direction within the IrO_6 octahedra. The ordered moment reaches 0.66(3)μ_B/Ir, larger than other iridates that form corner- or edge-sharing IrO_6 octahedral networks. Most importantly, the local environment of IrO_6 is close to the cubic limit and there is no direct connectivity between individual IrO_6 octahedra, making this system a canonical candidate to study the novel magnetism arising from the SOI.

II. EXPERIMENTAL RESULTS

Single crystals of CSIO were grown using a self-flux method similar to the one reported in Ref. [18], from off-stoichiometric quantities of IrO_2, $CaCO_3$, and $SrCO_3$ that were mixed with $CaCl_2$ and/or $SrCl_2$. The starting ratio of Ir to (Ca,Sr) is approximately 1:5. The mixed powders were fired to 1460 °C for 4 h and then slowly cooled at a rate of 4 °C/h. The compositions were independently checked to be consistent using both energy-dispersive x-ray analysis (EDX) (Hitachi/Oxford 3030 Plus) and single-crystal x-ray diffraction. The magnetic susceptibility and specific heat were measured using a

*yef1@ornl.gov

†Present address: National High Magnetic Field Laboratory, Tallahassee, FL 32306, USA.

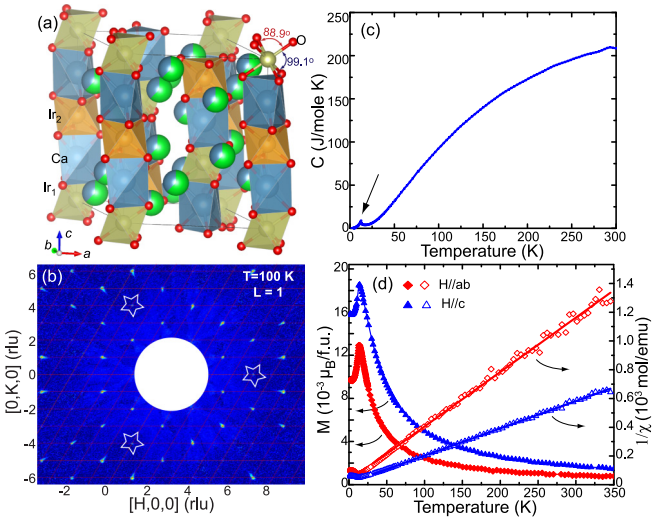

FIG. 1. (a) Crystal structure of $Ca_2Sr_2IrO_6$ in SG $R\bar{3}$. There are two distinct Ir1 and Ir2 sites located at (0,0,0) and (0,0,0.5) with different bonding oxygen environment. The trigonal distortion of IrO_6 leads to out-of-plane 88.9° and in-plane 91.1° bond angles. The structure is drawn using VESTA software [23]. (b) The reciprocal-space image in the $(h,k,l = 1)$ scattering plane at 100 K with data collected from the TOPAZ diffractometer. The nuclear peaks in white stars are forbidden reflections of SG $R\bar{3}c$. (c) Temperature dependence of specific heat $C_p(T)$. (d) T dependence of magnetization $M(T)$ and inverse magnetic susceptibility $1/\chi(T)$ in an applied magnetic field of 0.5 T parallel to the ab plane and the c axis in the field-cooling protocol. Solid lines are fits using the Curie-Weiss law above the transition temperature.

Quantum Design Magnetic Property Measurement System. X-ray diffraction data were collected using a Rigaku XtaLAB PRO diffractometer at the Oak Ridge National Laboratory (ORNL). A molybdenum anode was use to generate x ray with wavelength $\lambda = 0.7107$ Å. Neutron diffraction measurement was carried out using the TOPAZ diffractometer with a crystal size of $1 \times 1 \times 1.5$ mm^3 at the Spallation Neutron Source (SNS), ORNL. A larger piece with dimensions $1.5 \times 1.5 \times 4$ mm^3 was chosen for magnetic structure determination using the single-crystal diffuse scattering diffractometer CORELLI at SNS [19]. The $\pm 28.5°$ vertical angular coverage of the detector allows an extensive survey in reciprocal space. A 5 T vertical field superconducting magnet was used to study the field evolution of the spin structure.

Pure and Sr-doped Ca_4IrO_6 were reported to crystallize in a rhombohedral, K_4CdCl_6-type structure with $R\bar{3}c$ space group (SG No. 167) from x-ray powder diffraction studies [20]. The lattice parameters increase monotonically with Sr doping. The values become $a = b = 9.588$ Å and $c = 11.414$ Å for CSIO at room temperature. The crystal structure in Fig. 1(a) shows the one-dimensional (1D) chains of alternating IrO_6 octahedra and CaO_6 trigonal prisms parallel to the c axis. The single-crystal x-ray diffraction measurement on CSIO reveals that the majority of reflections are consistent with the reported $R\bar{3}c$ space group, with a significant portion of peaks violating the reflection conditions [345 out of 3152 reflections with $I > 3\sigma(I)$]. To further confirm the finding, we employed single-crystal neutron diffraction to characterize the structure. Figure 1(b) presents a typical contour plot in the $(h,k,l = 1)$ scattering plane. Indeed, several marked reflections cannot be indexed using SG 167, which requires both $h + l = 3n$ and $l = 2n$ in the $(h\bar{h}0l)$ scattering plane. The presence of (4,0,1) in Fig. 1(b) clearly indicates the breakdown of the reflection condition and suggests a reduced crystal structure symmetry. Based on the x-ray and neutron observation, the maximal nonisomorphic subgroup $R\bar{3}$ (No. 148) that lacks the c-axis glide is the most likely space group, where the unique Ir site (6b site in SG 167) splits into 3a and 3b Wyckoff positions. Such different surrounding oxygen environments allow the two Ir sites to have independent spin orientations. Each IrO_6 octahedron contains six identical Ir-O bond lengths of 2.036 Å. There is a small trigonal distortion with the octahedron stretched along the c axis; the corresponding O-Ir1-O and O-Ir2-O bond angles at 100 K are 88.92(8)° and 88.68(8)°, respectively. The overall local environment surrounding the Ir atoms is close to the ideal cubic limit. Furthermore, kaline earth atoms connecting neighboring IrO_6 along the c axis are dominated by Ca ions, while the sites between the IrO_6/CaO_6 chains have mixed Sr:Ca ions with a 2:1 ratio [Fig. 1(a)]. This atomic arrangement is probably due to the longer distance from the mixed site to the oxygen atoms, which is more suitable to host the larger Sr ions. This feature also agrees with a 2.7% increase in a but only a 1.6% increase in c from Ca_4IrO_6 to CSIO. It is noteworthy that the formation of two distinct octahedral sites is not common in the K_4CdCl_6-type compounds. The observation of the $R\bar{3}$ space group in CSIO might be related to the preferred site occupancy of the mixed Ca/Sr ions. It is certainly interesting to verify whether this is the case in similar material with the $R\bar{3}$ space group discovered in the future.

Figure 1(c) shows the T dependence of the specific heat of CSIO single crystal. A sharp anomaly appears near 13 K, indicating a magnetic transition similar to pure Ca_4IrO_6 [18,21]. Figure 1(d) shows the temperature evolution of the magnetic susceptibility χ with an applied magnetic field of 0.5 T. The peaks observed around 13.5 K confirm the phase transition. Fits of $1/\chi_{ab}$ ($1/\chi_c$) for $30 < T < 300$ K to a Curie-Weiss law yield effective magnetic moments μ_{eff} of 1.25 (2.14)μ_B and Curie temperatures θ_{CW} of -0.13 (-12.69) K for the field applied in the basal plane (parallel to the c axis). The negative value in θ_{CW} implies AFM interactions between the neighboring Ir ions. The large difference in both μ_{eff} and θ_{CW} within the ab plane and along the c axis indicates strong anisotropy in magnetic property and is consistent with the chainlike topology of the crystal structure. The average value $(2/3\theta^{ab}_{\text{CW}} + 1/3\theta^{c}_{\text{CW}})$ agrees well with the powder sample, where θ_{CW} decreases steadily with Sr doping [20]. For systems with a trigonal or triangular lattice, it is generally expected that there is a certain amount of magnetic frustration [22]. However, the small value of the frustration parameter ($\theta_{\text{CW}}/T_N \approx 0.32$) implies it is absent in CSIO.

The spin structure of CSIO in a zero applied magnetic field ($H = 0$) was characterized by surveying a large portion of the reciprocal volume at 5 K. The sample was oriented with the c axis perpendicular to the horizontal scattering plane. The diffraction data were collected with the crystal rotating along the c axis for 210°. Earlier studies of undoped Ca_4IrO_6 reported a spin configuration with a magnetic wave

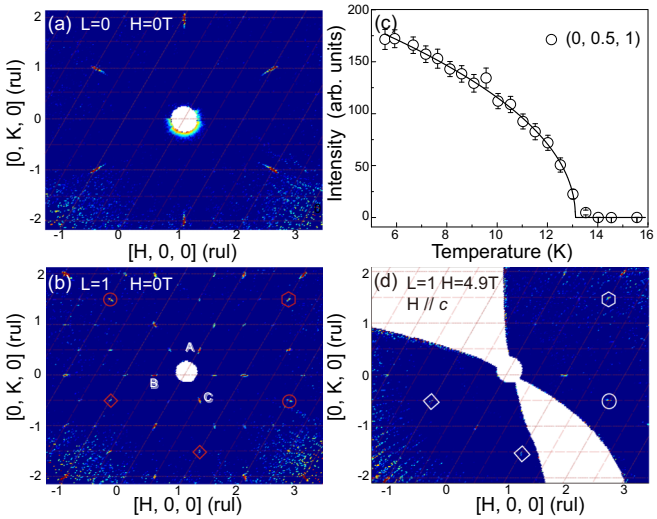

FIG. 2. The diffraction image in the (a) $(h,k,l=0)$ and (b) $(h,k,l=1)$ scattering plane at 5 K with zero field. A, B, and C label the three magnetic domains. Reflections encircled in squares, circles, and hexagons are from the same magnetic domain with the wave vector $q_m = (0,0.5,1)$. (c) T dependence of the (0,0.5,1) magnetic peak. The solid line is the fit of integrated intensity. (d) The image in the $(h,k,l=1)$ scattering plane with a magnetic field of $H = 4.9$ T applied along the c axis. The marked peaks are the magnetic reflections.

vector $q_m = (0.5,0.5,0)$ [21]. As shown in Fig. 2(a), the low-T contour plot in the $(h,k,l=0)$ scattering plane does not show extra intensities at this reflection and equivalent positions. In contrast, new reflections appear in the plane with $l = 2n+1$. All observed magnetic reflections at $(h,k,l=1)$ can be indexed using a magnetic wave vector $q_m = (0,0.5,1)$ plus two additional magnetic domains $-120°$ and $120°$ apart [Fig. 2(b)]. The volume fraction ratio of the three magnetic domains is 35:33:32, and is consistent with the trigonal symmetry. The observed magnetic propagation wave vector (0,0.5,1) in CSOI is the same as the isostructural Sr_3ZnIrO_6 [24]. The T dependence of the strongest magnetic reflection shows a clear second-order phase transition. Fitting the data using $I \sim (1 - T/T_N)^{2\beta}$ yields $T_N = 13.1(3)$ K and $\beta = 0.25(1)$. The value of β deviates from the critical exponent of a 3D spin system but is consistent with pure Ca_4IrO_6 [21].

The magnetic structure of CSIO is determined by analyzing over 80 reflections in conjunction with representational analysis [25]. For the SG $R\bar{3}$ with two inequivalent Ir sites and a propagation wave vector (0,0.5,1), the spin configuration is described by an irreducible representation (IR) that allows moments of Ir1(Ir2) along all three crystallographic axes. The relative phase between the two iridium sites could either be ferromagnetic (FM) or AFM. In the former case, one expects strong magnetic reflections in the scattering plane with l equal to even numbers. However, all major magnetic peaks are observed in the scattering plane with l equal to odd numbers, indicating a dominant AFM coupling between the two iridium sites. This feature is verified using the simulated annealing method [25]. There are weak peaks in the $l = 0$ plane, e.g., the (2,0.5,0) peak. This indicates that the spins at those two sites are not exactly out of phase, and

TABLE I. The basis vectors (BV) and refined spin components for the SG $R\bar{3}$ with $q_m = (0,0.5,1)$. Two independent Ir sites are located at (0,0,0) and (0,0,1/2), respectively.

IR	BV	Atom	m_a	m_b	m_c
Γ_1	ψ_1	Ir1	1	0	0
	ψ_2	Ir1	0	1	0
	ψ_3	Ir1	0	0	1
Γ_1	ψ_1	Ir2	1	0	0
	ψ_2	Ir2	0	1	0
	ψ_3	Ir2	0	0	1
	Refinement ($T = 5$ K)		$m_a(\mu_B)$	$m_b(\mu_B)$	$m_c(\mu_B)$
		Ir1	−0.33(2)	−0.64(2)	0.41(5)
		Ir2	0.32(2)	0.63(2)	−0.34(5)

it further confirms the reduced crystal symmetry. A reliable refinement of the spin configuration can only be reached by collecting a complete set of magnetic reflections in reciprocal space with domain populations correctly refined, since certain reflections result from the summation of different domains. Full details are given in the Supplemental Material [26]. Using the symmetry-adapted model and the magnetic form factor for Ir^{4+} [27], we obtained the spin structure with detailed information listed in Table I. As illustrated in Figs. 3(a)–3(b), the spins have staggered $+-$ patterns between neighboring sites along the c axis. The in-plane spin configuration is highly anisotropic despite the trigonal symmetry of the lattice. The moments are coupled ferromagnetically along the a axis but are antiferromagnetic along the b axis. The spin moments are dominantly aligned within the ab plane with an out-of-plane tilt angle of 34° toward the c axis. The projection in the

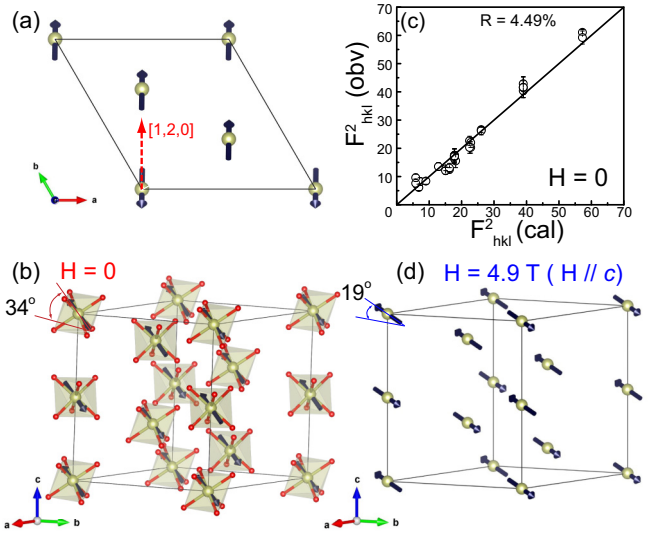

FIG. 3. (a) The spin configuration projected on the ab plane with the moment along the [1,2,0] direction. (b) The refined magnetic structure at $H = 0$ from single-crystal neutron diffraction measurement; the spin moments tilt 34° away from the ab plane. (c) The calculated magnetic intensities vs observation using the model described in the text. (d) The magnetic structure with $H = 4.9$ T applied along the c axis; the canting angle away from the basal plane reduces to 19°.

basal plane is parallel to the [1,2,0] direction. The moment direction is close to the diagonal O-Ir-O bond within the IrO_6. The nearly collinear spin configuration is in contrast with the noncollinear spin order reported in the isostructural Sr_3ZnIrO_6 [24]. The ordered moment in CSIO is $0.66(3)\mu_B$/Ir site. It is larger than other iridate compounds with corner- or edge-sharing IrO_6 octahedra [15,28–32], but comparable with the value of $0.87\mu_B$/Ir in Sr_3ZnIrO_6 and $0.6\mu_B$/Ir in the transition metal element substituted Sr_3CoIrO_6 that has a similar crystal structure with quasi-1D chains along the c axis [24,33]. Thus, the relative large ordered moment is most likely due to the suppressed electron hopping between the isolated IrO_6 octahedra.

The magnetic-field effect on the spin structure is investigated with a field applied along the c axis. The diffraction pattern in the $(h,k,l=1)$ scattering plane is presented in Fig. 2(d). Compared to the zero-field data, only one of the three magnetic domains survives at $H = 4.9$ T. This supports the conclusion that the observed magnetic reflections at $H = 0$ result from multiple domains instead of one single magnetic domain with multi-k structure [34]. A limited number of magnetic reflections are collected due to the partial block of a neutron beam by the magnet. With the spin configuration constrained to be similar to that at $H = 0$, the refined spins tilt further toward to the basal plane with a canting angle of 19°, and the ordered magnetic moment decreases to $0.60(7)\mu_B$/Ir [Fig. 3(d)]. The tilting of the moment direction toward to the basal plane is expected since the state with field H perpendicular to the easy magnetization is energetically more favorable. On the other hand, the absence of a spin-flip transition with field up to 4.9 T (the transition temperature T_N reduces from 12.5 K at $H = 0$ to 10.6 K at $H = 14$ T from specific-heat measurement) indicates the magnetic structure is rather robust and consistent with observations in other iridates [15].

To further understand the nature of the observed magnetic ordering, we performed density functional theory (DFT) calculations using the Vienna Ab initio Simulation Package VASP [35,36] with the modified Perdew-Burke-Ernzerhof exchange correlation designed for solids (PBEsol) [37]. We employed PAW potentials [38] with the following electronic configurations: Ca:$3p^6 3s^2$, Sr:$4s^2 4p^6 5s^2$, Ir:$6s^1 5d^8$, and O:$2s^2 2p^4$. The cation arrangement was chosen using a random number generator to assign Ca or Sr with the correct distribution on each site. The calculations were found to be converged with a 500 eV cutoff. To allow for the two antiferromagnetic configurations to be studied in a commensurate unit cell, $2 \times 2 \times 1$ unit cells were employed with a $1 \times 1 \times 2$ Monkhorst-Pack k-point mesh. All ionic coordinates were relaxed until all Hellmann-Feynman forces were less than 0.015 eV/Å. A Hubbard U of 2.0 eV and intrasite Hund's coupling $J_H = 0.2$ eV for Ir d-states were employed [39]. The magnetic structure shown in Fig. 3 (AFM3 state) and the one reported for pure Ca_4IrO_6 [AFM1 state with $q_m = (0.5,0.5,0)$ as shown in Ref. [21]] were chosen as the initial magnetic configurations. With SOI taken into account, the density of states (DOS) for both magnetic structures exhibit similar features. However, the energy of the AFM3 state is 2.5 meV/Ir site lower than that of AFM1 state, thereby confirms the observed magnetic structure as the most probable ground state. The initial magnetic structure tested in the calculation has the moments direction arbitrarily chosen

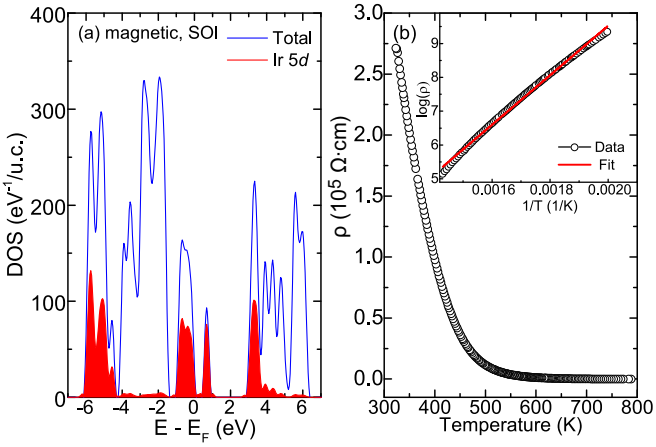

FIG. 4. The density of states of CSIO from DFT calculation with spin-orbit interaction included. The initial magnetic structure is similar to the one illustrated in Fig. 3. (b) The temperature dependence of resistivity of CSIO. The inset shows the fit to $\rho(T) = \rho_0 \exp(\Delta_{ag}/k_B T)$ with $\Delta_{ag} = 0.63$ eV.

while keeping the configuration consistent with the magnetic wave vector, but the converged state has moments relaxed nearly along the Ir-O bond direction. There is an insulating gap ~0.5 eV near E_F, mainly from the t_{2g} orbital of the Ir^{5+} ions. This is consistent with the resistivity measurement shown in Fig. 4(b), where a band gap $(2\Delta_{ag}) \sim 1.26$ eV is obtained by fitting the data to the form of $\rho(T) = \rho_0 \exp(\Delta_{ag}/k_B T)$ for $300 < T < 500$ K. The calculated spin moment of $0.5\,\mu_B$/Ir agrees well with the experimental observation.

III. DISCUSSION

The anisotropic magnetic configuration that breaks the trigonal symmetry and the moment direction following the diagonal O-Ir-O bond strongly suggests the emergence of relativistic SOI, where the exact form of the magnetic Hamiltonian depends on the lattice geometry [9]. A Heisenberg interaction $\vec{S}_i \cdot \vec{S}_j$ dominates in a corner-shared iridate, e.g., the square lattice Sr_2IrO_4. The canted spin moments that rigidly follow the staggered rotation of octahedra [30,40] are naturally explained by the strong SOI. In contrast, the highly anisotropic interactions appear due to the off-diagonal hopping matrix in the edge-shared case. This maps the system into a quantum compass model and has been studied extensively in the honeycomb lattice A_2IrO_3 [41,42]. Since the building blocks of perovskite-derived iridates are made of individual IrO_6 octahedrons, the isolated IrO_6 without corner- or edge-sharing connectivity makes the CSIO an ideal system to study the SOI in the single-ion limit. On the other hand, the influence of nonoctahedral crystal-field splitting (Δ) cannot be ignored. Although the $j_{\text{eff}} = 1/2$ state was initially thought to be a robust feature in iridates, as evidenced by the vanishing intensity at the L_2 absorption edge [3], it is now recognized that the local distortion could dramatically modify the ground states. For example, RIXS measurements on a quasi-one-dimensional spin chain Sr_3CuIrO_6 have revealed $\Delta = 0.31$ eV caused by the reduction of the O-Ir-O bond angle to 82°, and they contributed a significant mixing between $j_{\text{eff}} = 1/2$ and 3/2 states [16].

A similar result is reported in postperovskite $CaIrO_3$ [17], where the energy scale of the octahedral compression along the local z axis ($\Delta = -0.71$ meV) is comparable with the SOI strength $\lambda = 0.52$ meV and signifies a departure from the $j_{\text{eff}} = 1/2$ state. While the local symmetry of these compounds is not the same, i.e., tetragonal for perovskites and trigonal for nonperovskites, distortions of the IrO_6 octahedron seem to be ubiquitously present in the so-called $j_{\text{eff}} = 1/2$ iridates (e.g., Na_2IrO_3 with $|\Delta| = 0.11$ eV [43], $Y_2Ir_2O_7$ with $|\Delta| = 0.59$ eV [44]). A nonoctahedral crystal field must be considered in realistic models since the electronic structure is highly dependent on the relative orbital contributions. In this respect, the A_4BO_6 (A denotes alkaline earth ions and B is a $4d$ or $5d$ element) system featuring a chainlike structure with minimal local distortion of BO_6 octahedra represents a new family of platforms to realize the spin-orbit-entangled state. Yet, distinct magnetic configurations have been reported in isostructural iridates such as spin order with wave vector (0.5,0.5,0) in Ca_4IrO_6 [21], or a noncollinear spin structure in Sr_3ZnIrO_6 [24]. The difference indicates that the magnetic coupling between seemingly isolated Ir octahedra might depend on the overall averaged lattice and warrant more experimental investigation. Unlike the transition metal substituted Sr_3NiIrO_6 or Sr_3CoIrO_6, where the magnetism is influenced by the interplay between the transition metal and the $5d$ ions, or the $4d$ counterpart Sr_4RhO_6 [45], where the strength of SOI is smaller than the $5d$ systems, the CSIO can be regarded as a suitable example to further explore the electronic and magnetic properties arising from the SOI.

In summary, neutron and x-ray diffraction have been employed to investigate the crystal and magnetic structures of the trigonal lattice iridate $Ca_2Sr_2IrO_6$. The well-separated IrO_6 octahedra are close to the cubic limit with six equal Ir-O bond distances and O-Ir-O bond angles $\approx 90^\circ$. The Ir^{4+} spins form an anisotropic three-dimensional antiferromagnetic configuration with wave vector (0,0.5,1). The ordered moment is $0.66(3)\mu_B$/Ir, which is larger than iridates with corner- and edge-sharing IrO_6 octahedral networks. The DFT calculation confirms that the observed magnetic ordering is the most probable ground state and indicates that the insulating behavior is enhanced by the spin-orbit interaction.

The Department of Energy will provide public access to these results of federally sponsored research in accordance with the DOE Public Access Plan [46].

ACKNOWLEDGMENTS

We thank G. Jackeli and J. M. Perez-Mato for stimulating discussion. Research at ORNL's SNS was sponsored by the Scientific User Facilities Division, Basic Energy Sciences, U.S. Department of Energy (DOE). Theoretical calculations were supported by the Materials Sciences and Engineering Division (SO), Office of Basic Energy Sciences, U.S. DOE, and through the Office of Science Early Career Research Program (VRC). Computing resources are from NERSC, supported by the office of science, U.S. DOE under Contract No. DE-AC02-05CH11231. Work at the University of Colorado was supported by the U.S. National Science Foundation via Grant No. DMR-1712101. J.M.S. acknowledges support from China Scholarship Council.

This manuscript has been authored by UT-Battelle, LLC under Contract No. DE-AC05-00OR22725 with the U.S. Department of Energy. The United States Government retains and the publisher, by accepting the article for publication, acknowledges that the U.S. Government retains a nonexclusive, paid-up, irrevocable, worldwide license to publish or reproduce the published form of this manuscript, or allow others to do so, for United States Government purposes.

[1] B. J. Kim, H. Jin, S. J. Moon, J. Y. Kim, B. G. Park, C. S. Leem, J. Yu, T. W. Noh, C. Kim, S. J. Oh, J. H. Park, V. Durairaj, G. Cao, and E. Rotenberg, Phys. Rev. Lett. **101**, 076402 (2008).

[2] S. J. Moon, H. Jin, K. W. Kim, W. S. Choi, Y. S. Lee, J. Yu, G. Cao, A. Sumi, H. Funakubo, C. Bernhard, and T. W. Noh, Phys. Rev. Lett. **101**, 226402 (2008).

[3] B. J. Kim, H. Ohsumi, T. Komesu, S. Sakai, T. Morita, H. Takagi, and T. Arima, Science **323**, 1329 (2009).

[4] D. Pesin and L. Balents, Nat. Phys. **6**, 376 (2010).

[5] A. Shitade, H. Katsura, J. Kunes, X. L. Qi, S. C. Zhang, and N. Nagaosa, Phys. Rev. Lett. **102**, 256403 (2009).

[6] Y. Okamoto, M. Nohara, H. Aruga-Katori, and H. Takagi, Phys. Rev. Lett. **99**, 137207 (2007).

[7] F. Wang and T. Senthil, Phys. Rev. Lett. **106**, 136402 (2011).

[8] H. Watanabe, T. Shirakawa, and S. Yunoki, Phys. Rev. Lett. **110**, 027002 (2013).

[9] G. Jackeli and G. Khaliullin, Phys. Rev. Lett. **102**, 017205 (2009).

[10] C. C. Price and N. B. Perkins, Phys. Rev. Lett. **109**, 187201 (2012).

[11] Y. Singh, S. Manni, J. Reuther, T. Berlijn, R. Thomale, W. Ku, S. Trebst, and P. Gegenwart, Phys. Rev. Lett. **108**, 127203 (2012).

[12] N. Taira, M. Wakeshima, and Y. Hinatsu, J. Phys. Condens. Matter **13**, 5527 (2001).

[13] M. K. Crawford, M. A. Subramanian, R. L. Harlow, J. A. Fernandez-Baca, Z. R. Wang, and D. C. Johnston, Phys. Rev. B **49**, 9198 (1994).

[14] S. K. Choi, R. Coldea, A. N. Kolmogorov, T. Lancaster, I. I. Mazin, S. J. Blundell, P. G. Radaelli, Y. Singh, P. Gegenwart, K. R. Choi, S. W. Cheong, P. J. Baker, C. Stock, and J. Taylor, Phys. Rev. Lett. **108**, 127204 (2012).

[15] F. Ye, S. Chi, H. Cao, B. C. Chakoumakos, J. A. Fernandez-Baca, R. Custelcean, T. F. Qi, O. B. Korneta, and G. Cao, Phys. Rev. B **85**, 180403 (2012).

[16] X. Liu, V. M. Katukuri, L. Hozoi, W.-G. Yin, M. P. M. Dean, M. H. Upton, J. Kim, D. Casa, A. Said, T. Gog, T. F. Qi, G. Cao, A. M. Tsvelik, J. van den Brink, and J. P. Hill, Phys. Rev. Lett. **109**, 157401 (2012).

[17] M. M. Sala, K. Ohgushi, A. Al-Zein, Y. Hirata, G. Monaco, and M. Krisch, Phys. Rev. Lett. **112**, 176402 (2014).

[18] G. Cao, V. Durairaj, S. Chikara, S. Parkin, and P. Schlottmann, Phys. Rev. B **75**, 134402 (2007).

[19] F. Ye, Y. Liu, R. Whitfield, R. Osborn, and S. Rosenkranz, J. Appl. Crystallogr. **51**, 315 (2018).

[20] N. Segal, J. F. Vente, T. S. Bush, and P. D. Battle, J. Mater. Chem. **6**, 395 (1996).
[21] S. Calder, G. X. Cao, S. Okamoto, J. W. Kim, V. R. Cooper, Z. Gai, B. C. Sales, M. D. Lumsden, D. Mandrus, and A. D. Christianson, Phys. Rev. B **89**, 081104 (2014).
[22] A. P. Ramirez, Annu. Rev. Mater. Sci. **24**, 453 (1994).
[23] K. Momma and F. Izumi, J. Appl. Crystallogr. **44**, 1272 (2011).
[24] P. A. McClarty, A. D. Hillier, D. T. A. D. D. Khalyavin, S. Rayaprol, P. Manuel, W. Kockelmann, and E. V. Sampathkumaran, arXiv:1610.00038.
[25] J. Rodriguez-Carvajal, Physica B **192**, 55 (1993).
[26] See Supplemental Material at http://link.aps.org/supplemental/10.1103/PhysRevB.97.235116 for further details of crystal and magnetic structure characterization.
[27] K. Kobayashi, T. Nagao, and M. Ito, Acta Crystallogr. A **67**, 473 (2011).
[28] G. Cao, J. E. Crow, R. P. Guertin, P. F. Henning, C. C. Homes, M. Strongin, D. N. Basov, and E. Lochner, Solid State Commun. **113**, 657 (2000).
[29] S. W. Lovesey, D. D. Khalyavin, P. Manuel, L. C. Chapon, G. Cao, and T. F. Qi, J. Phys. Condens. Matter **24**, 496003 (2012).
[30] F. Ye, S. Chi, B. C. Chakoumakos, J. A. Fernandez-Baca, T. Qi, and G. Cao, Phys. Rev. B **87**, 140406 (2013).
[31] C. Dhital, S. Khadka, Z. Yamani, C. de la Cruz, T. C. Hogan, S. M. Disseler, M. Pokharel, K. C. Lukas, W. Tian, C. P. Opeil, Z. Q. Wang, and S. D. Wilson, Phys. Rev. B **86**, 100401 (2012).
[32] C. Dhital, T. Hogan, Z. Yamani, C. de la Cruz, X. Chen, S. Khadka, Z. Ren, and S. D. Wilson, Phys. Rev. B **87**, 144405 (2013).
[33] D. Mikhailova, B. Schwarz, A. Senyshyn, A. M. T. Bell, Y. Skourski, H. Ehrenberg, A. A. Tsirlin, S. Agrestini, M. Rotter, P. Reichel, J. M. Chen, Z. Hu, Z. M. Li, Z. F. Li, and L. H. Tjeng, Phys. Rev. B **86**, 134409 (2012).
[34] S. V. Gallego, J. M. Perez-Mato, L. Elcoro, E. S. Tasci, R. M. Hanson, K. Momma, M. I. Aroyo, and G. Madariaga, J. Appl. Crystallogr. **49**, 1750 (2016).
[35] G. Kresse and J. Furthmüller, Comput. Mater. Sci. **6**, 15 (1996).
[36] G. Kresse and J. Furthmüller, Phys. Rev. B **54**, 11169 (1996).
[37] J. P. Perdew, A. Ruzsinszky, G. I. Csonka, O. A. Vydrov, G. E. Scuseria, L. A. Constantin, X. Zhou, and K. Burke, Phys. Rev. Lett. **100**, 136406 (2008).
[38] P. E. Blöchl, Phys. Rev. B **50**, 17953 (1994).
[39] S. L. Dudarev, G. A. Botton, S. Y. Savrasov, C. J. Humphreys, and A. P. Sutton, Phys. Rev. B **57**, 1505 (1998).
[40] S. Boseggia, H. C. Walker, J. Vale, R. Springell, Z. Feng, R. S. Perry, M. M. Sala, H. M. Ronnow, S. P. Collins, and D. F. McMorrow, J. Phys. Condens. Matter **25**, 422202 (2013).
[41] J. Chaloupka, G. Jackeli, and G. Khaliullin, Phys. Rev. Lett. **110**, 097204 (2013).
[42] J. G. Rau, E. K.-H. Lee, and H.-Y. Kee, Phys. Rev. Lett. **112**, 077204 (2014).
[43] H. Gretarsson, J. P. Clancy, X. Liu, J. P. Hill, E. Bozin, Y. Singh, S. Manni, P. Gegenwart, J. Kim, A. H. Said, D. Casa, T. Gog, M. H. Upton, H.-S. Kim, J. Yu, V. M. Katukuri, L. Hozoi, J. van den Brink, and Y.-J. Kim, Phys. Rev. Lett. **110**, 076402 (2013).
[44] L. Hozoi, H. Gretarsson, J. P. Clancy, B. G. Jeon, B. Lee, K. H. Kim, V. Yushankhai, P. Fulde, D. Casa, T. Gog, J. Kim, A. H. Said, M. H. Upton, Y.-J. Kim, and J. van den Brink, Phys. Rev. B **89**, 115111 (2014).
[45] S. Calder, L. Li, S. Okamoto, Y. Choi, R. Mukherjee, D. Haskel, and D. Mandrus, Phys. Rev. B **92**, 180413 (2015).
[46] http://energy.gov/downloads/doe-public-access-plan